Gelation and phase coexistence in colloidal suspensions with short-range forces: Generic behavior versus specificity

Ph. Germain and S. Amokrane

Physique des Liquides et Milieux Complexes, Faculté des Sciences et Technologie, Université Paris Est (Créteil), 61 Avenue du Général de Gaulle, 94010 Créteil Cedex, France

(Received 24 June 2009; revised manuscript received 31 August 2009; published 20 January 2010)

The interplay between physical gelation and equilibrium phase transitions in asymmetric binary mixtures is analyzed from the effective fluid approach, in which the big particles interact via a short-range effective attraction beyond the core due to the depletion mechanism. The question of the universality of the scenario for dynamical arrest is then addressed. The comparison of the phase diagrams of the hard-sphere mixture and the Asakura-Oosawa models at various size ratios shows that strong specificity is observed for nonideal depletants. In particular, equilibrium gelation, without the competition with fluid-fluid transition is possible in mixtures of hard-sphere colloids. This is interpreted from the specificities of the effective potential, such as its oscillatory behavior and its complex variation with the physical parameters. The consequences on the dynamical arrest and the fluid-fluid transition are then investigated by considering in particular the role of the well at contact and the first repulsive barrier. This is done for the actual effective potential in the hard-sphere mixture and for a square well and shoulder model, which allows a separate discussion of the role of the different parameters, in particular on the localization length and the escape time. This study is next extended to mixtures of "hard-sphere-like" colloids with residual interactions. It confirms the trends relative to equilibrium gelation and illustrates a diversity of the phase behavior well beyond the scenarios expected from simple models.

DOI: 10.1103/PhysRevE.81.011407 PACS number(s): 82.70.Dd, 64.70.Q−, 64.75.−g

I. INTRODUCTION

The question of gelation in colloids has attracted considerable interest in the past decade, both for practical and fundamental reasons. Besides the presence of colloidal gels in a variety of situations, from industrial processes to everyday life, colloids provide indeed convenient model systems for studying the glass transition, just as for the study of the equilibrium phase transitions. This is due to the possibility to tune to a certain extent the colloidal interactions (range, strength, anisotropy, etc.) controlling their thermodynamic properties. Concerning the dynamics, the extension to Brownian particles of the theoretical framework developed for molecular glasses has led to an original picture of the dynamical arrest [1,2]: in addition to the ordinary "repulsive" glass expected for fluids of hard particles ("caging" mechanism), colloidal suspensions can exhibit a transition to "attractive" ones when short-range attractions exist between the colloids [3–11] (see also [12,13] for a review). In such attractive glasses, the arrest is related to the existence of long-lived reversible bonds between the particles, induced by the effective attractions. Such reversible attractive glasses are usually referred to, at lower density, as physical gels [13]. Defined in a broad way, the short-range attractions responsible for this exist in a number of colloidal suspensions considered from the effective one-component fluid point of view, such as, for instance, in globular proteins [14,15], colloidal silica [16], or ideal polymer-colloid mixtures [5] (in this last case, for example, their physical origin is the well-known depletion effect). Early mode coupling theory (MCT) studies [3] have shown that fluids of attractive hard spheres (HS) can exhibit gelation when the attraction range is short enough in accord with experiment on various suspensions [5,6,14,16,17], and from a few years now, with numerical simulations [8,9,18].

An important question, both practical and fundamental, emerged from these studies. It concerns the interplay between gelation and the equilibrium phase transition. More specifically, as the effective attractions responsible for the gelation are also involved in equilibrium phase transitions, the possibility of observing physical gelation in the homogenous fluid phase, without an intervening phase separation, has been questioned [13,18–20]. The relevant phase coexistence is the fluid-fluid (FF) one since fluid-solid (FS) coexistence can be suppressed in practice by a certain amount of polydispersity. In a recent work we have proposed a new perspective on this question [21]. We have shown that at variance with some claims in the recent literature [13,19,20,22]—at least from the point of view of the effective one-component system—several scenarios should be considered in the answer. The usual view associating gelation to fluid phase condensation is indeed based on a particular description of the effective interactions between the colloids. In this description, the effective potential is essentially a hard-core repulsion plus a short-range attraction, with all the other details being irrelevant. The conclusions obtained from standard generic models, such as the square well (SW) or the Yukawa potential, are then extrapolated to all the suspensions in which an effective attraction exists [13] from theoretical conjectures concerning laws of corresponding states [23]. In this scheme, physical gelation would occur only through an interrupted FF phase separation (hereafter, this will be referred to as the generic scenario for physical gelation). This was deduced from numerical simulations performed on the SW potential [13,18], which showed that previous MCT results overestimated the domain of existence of the nonergodic state. Recent experimental results seemed to corroborate this view [15,20,22,24] although former studies were compatible with the alternative one [6,25,26]. In [21],

we illustrated on the very simple example of a binary mixture of hard spheres with different radii that the reduction in the effective interaction to a hard-core repulsion plus a short-range attraction can in fact be insufficient. Although—roughly speaking—such mixtures belong to the same generic category, the specificity of the HS effective potential is already sufficient to lead to a more complex scenario: beyond the hard core, one finds a primary depletion well whose characteristics (depth and width) depend on the physical parameters in a complex way. After this well, the potential is oscillatory at the scale of the smaller spheres, with the repulsive barriers playing also a role in the phenomenon of gelation. These features make possible, in some situations, the onset of equilibrium gelation, contrarily to other experimental situations [15,20,22,24]. Furthermore, as the FF transition can in turn be absent from the phase diagram, this even rules out the question of its competition with gelation. This shows that different scenarios can exist concerning gelation, and therefore a fine analysis is required for determining the appropriate modeling for each colloidal system.

In this paper we will extend this study in three main directions. In Sec. III, we will study more completely the influence of the size ratio on the binodals and the nonergodicity transition line of the HS mixture. A systematic comparison with the Asakura-Oosawa (AO) model will be made to assess the relative weights of the size asymmetry and the more specific features of the effective interaction. This will be helpful for determining the situations in which one would likely observe equilibrium gelation, without the competition of the fluid condensation. In Sec. IV, we will analyze in more detail the role of the repulsive barriers observed for nonideal depletants. We will use for this the flexible square and shoulder potential, which mimics some characteristics of the HS depletion potential and allows a separate analysis of the influence of the depth and width of the attractive well or the width and height of the barrier. Finally, we will examine in Sec. V mixtures of hard-sphere-like colloids in which very short-range interactions beyond the hard core are present, as this is likely in real mixtures. We will then confirm the situations in which equilibrium gelation can be expected experimentally. We will also illustrate on one example the possibility of complex behavior as, for instance, equilibrium gelation pre-empting both the FF and the FS transitions, various re-entrant phenomena or solid-solid (SS) transitions. This is followed by the general conclusion, with the computational methods being described in the next section.

II. METHODS

The methods we have used are detailed in our previous work [21,27]. We briefly recall here the main steps. The binodals and the nonergodicity transition lines are computed in the effective one-component representation of a binary mixture with big to small spheres diameter ratio $q=\sigma_b/\sigma_s>1$ and packing fractions (η_s,η_b). The thermodynamic variables are then the packing fraction of the big particles η_b, and that of the small ones in the reservoir η_s^* (also the temperature T for non-HS interactions). For hard particles without long-range forces, the effective fluid approximation leads to quite reasonable results [28–32] as far as the binodals are concerned. The structure is also correctly reproduced for diameters ratios down to $q=3$ [33]. The effective potential between the big particles is obtained from the infinite dilution limit $\rho_b\to 0$ of the pair distribution function (pdf) of the big particles g_{bb} [34,35],

$$\phi^{eff}(r) = -k_BT\ln[g_{bb}(r,\rho_b\to 0)] - u_{bb}(r), \tag{1}$$

where u_{22} is the direct potential between the big spheres. We used the reference hypernetted chain (RHNC) closure of Lado *et al.* [36] of the Ornstein-Zernike equations for the mixture with bridge functions deduced from Rosenfeld's density functional theory [37]. This method can be used also for non-HS potentials [38], including the very-short-range attractions used here for describing mixture of HS-like particles [39]. For the Asakura-Oosawa mixture, the potential of mean force at infinite dilution has the well-known exact expression (in unit of k_BT) [40,41],

$$\phi_{AO}(x) = \begin{cases} \infty, & x<1 \\ -\dfrac{\pi}{4}q^3\rho_s^*\left[\dfrac{2}{3}\left(1+\dfrac{1}{q}\right)^3 - x\left(1+\dfrac{1}{q}\right)^2 + \dfrac{x^3}{3}\right], & 1\le x\le 1+\dfrac{1}{q} \\ \infty, & x>1+\dfrac{1}{q} \end{cases} \tag{2}$$

with $\rho_s^*=(6/\pi\sigma_s^3)\eta_s^*$ the reduced solvent density in the reservoir. We also used the RHNC closure (with the bridge function of Malijevsky and Labik [42] for convenience) to compute the static structure and the free energy of the effective fluid. The free energy of the solid is computed from the variational perturbation theory (VPT) using standard parameterization of the reference HS solid [43]. This method allows for a quantitative description of the FF and the FS transitions. This was shown in [30] where the binodals and the free energy are compared to the Monte Carlo results of [28] for $q=5$, 10 (Figs. 2, 4, and 6; see also [29,31]). The pdf is also accurately reproduced with respect to numerical simu-

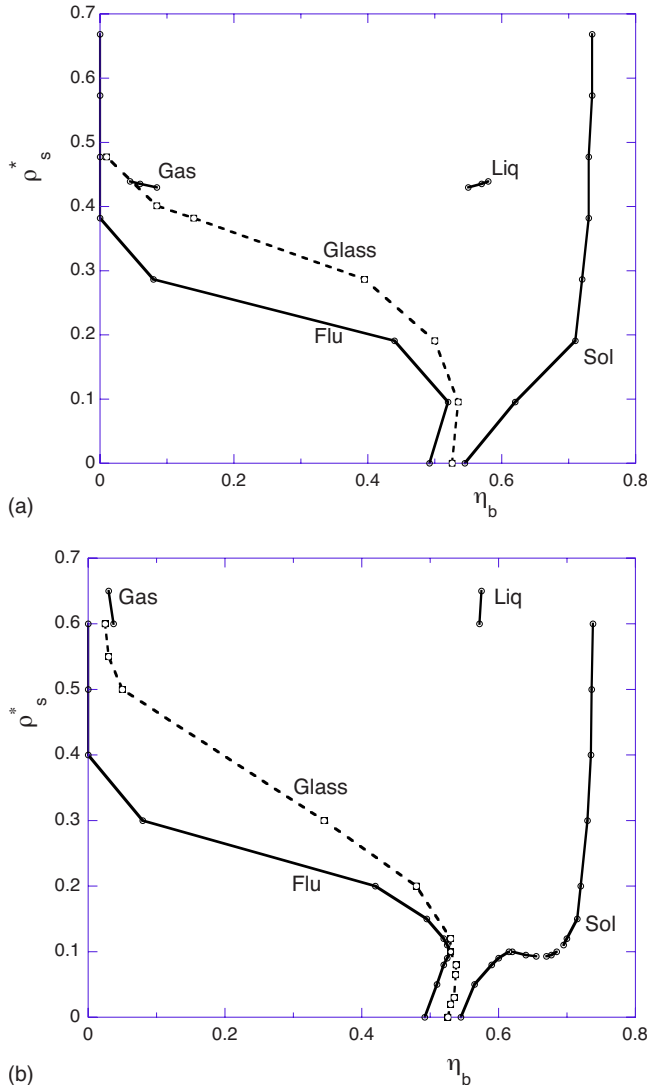

FIG. 1. (Color online) Phase diagram of the (a) Asakura-Oosawa and (b) hard-sphere mixture models for q=12.5 in the effective fluid representation. Solid lines: binodals; dashes: nonergodicity transition lines.

lations (see Fig. 1 of [30]). The VPT is less accurate for describing the extended solid at high solvent density, and thus a possible SS transition if the latter would exist in this region [a stable SS transition is attested at high asymmetry and relatively low ρ_s^* (see [28] and below)]. This point, however, is not central in our discussion.

The nonergodicity line is computed from the MCT [1] (for the derivation for colloids, see Ref. [2]). The relevant quantity is the density autocorrelation function whose long-time limit f_q characterizes the ergodicity of the fluid: $f_q \neq 0$ corresponds to the nonergodic or dynamically arrested state. f_q is the greatest solution, in the range $0 \leq f_q \leq 1$, of the equation [44]

$$\frac{f_q}{1-f_q} = \frac{1}{2}\int \frac{d^3k}{(2\pi)^3} V(q,k) f_k f_{|q-k|}, \tag{3}$$

where

$$V(\mathbf{q},\mathbf{k}) = -\frac{\rho_b}{q^4}[\mathbf{q}\cdot(\mathbf{q}-\mathbf{k})c_{|\mathbf{q}-\mathbf{k}|} + \mathbf{q}\cdot\mathbf{k}c_k]^2 S_q S_k S_{|\mathbf{q}-\mathbf{k}|} \tag{4}$$

with c_k the static direct correlation function and $S_k = 1/(1-\rho_b c_k)$ the static structure factor.

For one-component fluids, the MCT is known to describe correctly the repulsive and the attractive glass transition of the dense fluid [45–47], although its predicts a lower packing fraction at the glass transition than simulations (η=0.525 instead of η=0.58 in the second reference of [7]). Its main limitation concerns the description of the low density fluid ($\eta < 0.25$), where cluster aggregation is also observed [6,13] and the situations for which the system is close to a FF instability (this is the consequence of the approximate treatment of the density fluctuations, which does not account for such heterogeneities [3]). However, this should not invalidate the main results of this paper since in most situations we consider, such considerations are irrelevant. This concerns especially our main results concerning the possible suppression of the gelation-FF transition competition induced by the specificity of the effective potential. Another important aspect of the method is the choice of the static input S_k, as discussed in Ref. [27]. It is also clear that simulations would be useful to assess quantitatively the results for the dynamical arrest obtained from the one-component mode coupling theory. The validity of the effective fluid approach is indeed then less established than for the static properties. There exist only partial results for mixtures of soft particles [48], or comparison with simulations at low density of the small particles for AO mixtures [49], and theoretical arguments like the adiabadicity criterion [50]. The underlying view is that the fluid of small particles remains ergodic in the free volume left by the big ones, which seems to be a reasonable approximation for the situations investigated in this paper, that is, hard particles and $\eta_s^* \leq 0.4$. Quantitatively, however, an extension of the nonergodicity domain cannot be excluded in certain circumstances, with the gelation involving also the small particles. This was indeed observed by Imhof and Dhont [51] for a mixture of hard-sphere-like particles for the higher values of η_s^*, and it may be expected, for example, when additional attractions are present. In any case, this widening of the nonergodicity domain would just reinforce our conclusions concerning the possible existence of equilibrium gels in asymmetric mixtures. It should be stressed that the dynamical arrest has been characterized in the recent literature by other methods, such as the bond correlation [52] or percolation [53]. It is unclear how the arrest lines estimated in this way correlate with the one determined from the density autocorrelation function, central to this MCT treatment.

III. MIXTURES OF HARD PARTICLES

A. Results

In order to possibly draw general trends, we collect in Figs. 1–3 the phase diagrams of the HS and the AO mixtures [21,27] in the effective fluid approach, at different size ratios. Two situations may indeed be distinguished: highly asymmetric mixtures ($q \geq 10$) and moderately asymmetric ones (typically q=4,5). For q=12.5 and 10, the phase diagrams of

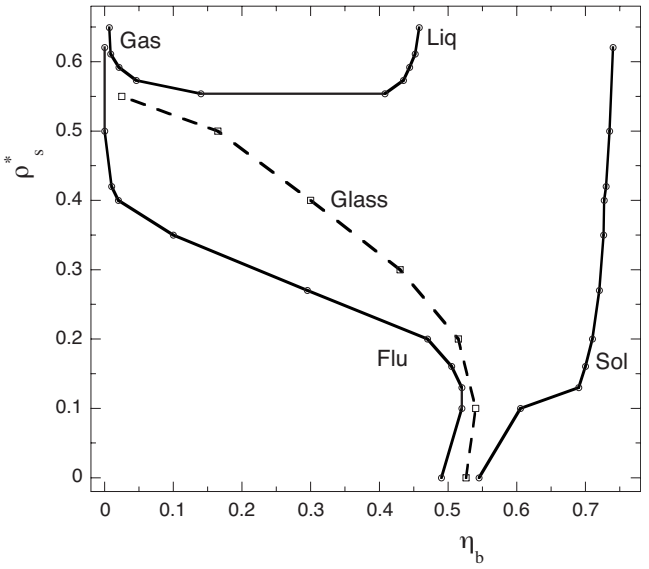

FIG. 2. Phase diagram of the HS mixture for $q=10$. Solid lines: binodals; dashes: nonergodicity transition lines.

the HS and the AO mixture are quite similar. We indeed observe (1) a wide FS coexistence domain which confines the homogenous fluid phase to the low solvent density region, $\rho_s^* \approx 0.2-0.3$; (2) a metastable FF binodal which also is very flat; and (3) the glass transition line pre-empting the FF one, at least according to this MCT approach. In both models, the nonergodicity domain expands toward lower packing fractions of the big particles η_b upon increasing the density of the small ones, beyond $\rho_s^* \approx 0.1$. This is associated with the transition to the attractive glass, as evidenced by the analysis of the nonergodicity factor f_q (see Sec. IV). As emphasized previously, the meaning of the MCT line at very low η_b needs to be clarified, as dynamical heterogeneities are not accounted for in the MCT which considers only homogenous gelation. The closeness of the FF critical point (at least for the AO model) should also be considered. Although these restrictions may be important in practice, they should not invalidate our analysis, which shows similar properties between the two models at large asymmetry. These similarities found within the same theoretical framework are indeed associated with the high asymmetry, as also substantiated by comparison with the lower asymmetry regime. Here, the unique qualitative difference is the existence, in a very narrow range of solvent densities, of a stable SS transition for the HS mixture model. More quantitatively, one also observes that the FF occurs at higher ρ_s^* for ϕ_{HS}^{eff} than for ϕ_{AO}.

For $q=4$, 5 the phase diagrams of the two models differ qualitatively. Besides the freezing line (less flat with ϕ_{HS}^{eff}), the most striking deviations concern the FF transition and the glassy states: the FF binodal is absent for ϕ_{HS}^{eff} (it appears only for $q>8$), while it is systematically observed in the AO mixture (it is stable with respect to the FS one for $q \leq 2.5$ [54,55]). Concerning the glassy state, it is confined to the dense liquid region ($\eta_b \sim 0.5$) with ϕ_{AO}, while it is observed at relatively at low density with ϕ_{HS}^{eff}. For the latter, "gelation" occurs at $\eta_g=0.32$ for $\rho_s^*=0.8$ and $q=5$, and $\eta_g=0.18$ for $q=8$ (still for $\rho_s^*=0.8$). In a recent numerical simulation

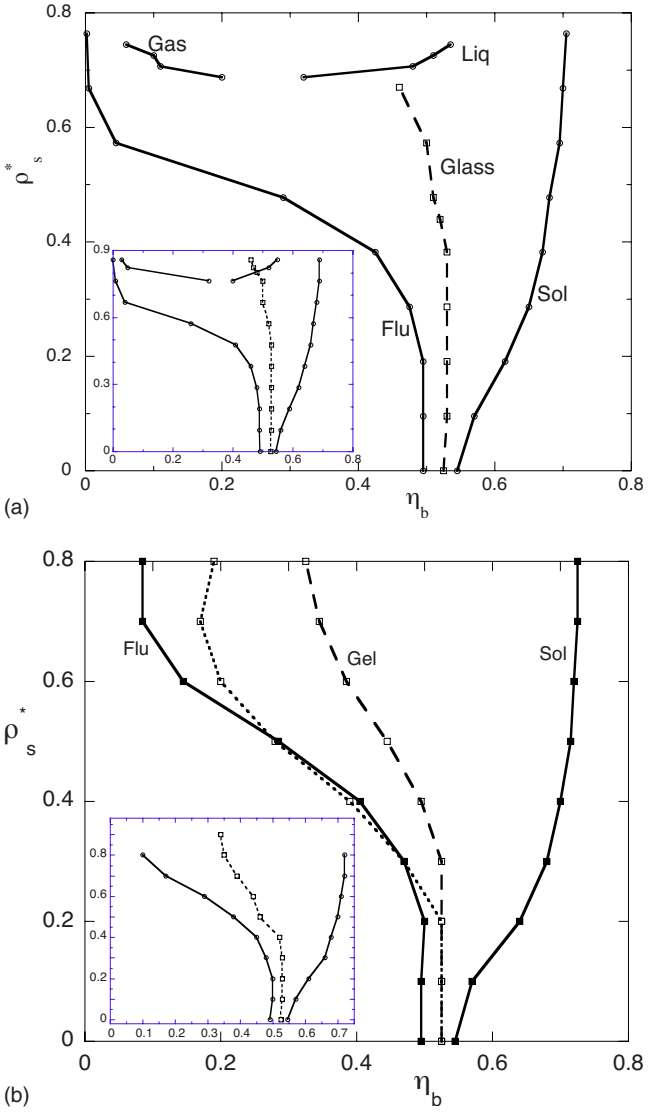

FIG. 3. (Color online) Same as Fig. 1 for $q=5$ (inset: $q=4$). The dots in (b) are the nonergodicity transition line for $q=8$ (note that the FF transition is absent for $q \leq 8$).

[52], the dynamical arrest was studied for the AO potential with $q^{-1}=0.15$ from the bond correlation function. At this size ratio arrest is observed at low packing fraction, but the location of the glass transition line was not computed.

For moderately asymmetric mixtures, the phase behavior observed with ϕ_{HS}^{eff} departs clearly from the generic scenario. One may then wonder whether a different representation would restore a common behavior. To check this we have considered the standard B_2 representation based on an assumed validity of certain laws of corresponding states. According to these laws the only relevant measure of the interaction strength would be the reduced second virial coefficient $B_2^r=(1/B_2^{HS})\int d^3\mathbf{r}\{1-\exp[-\beta\phi(r)]\}$. This was shown for the binodals in [23] for potentials having widely different ranges of attractive interactions, but the authors already indicated that discrepancies could be observed for more complex effective potentials such as those involving barriers. It was next suggested in [18] from simulations that the law of corresponding states could also hold for the dy-

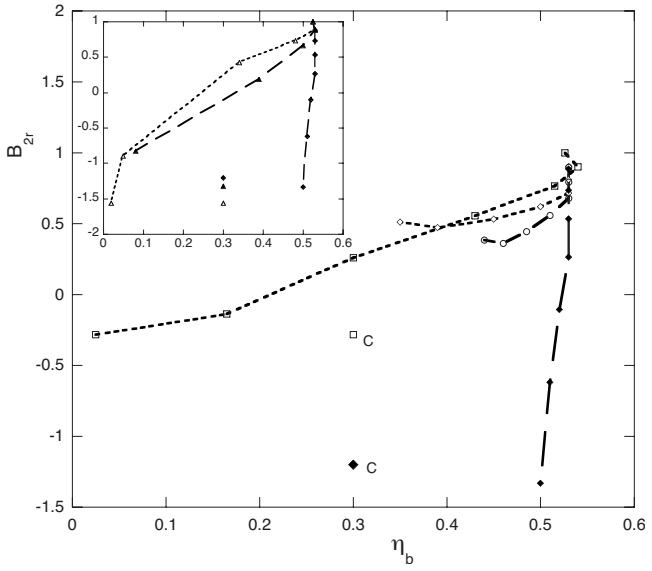

FIG. 4. Nonergodicity transition lines and FF critical points in the (η_b, B_{2r}) plane for different effective potentials. $q=5$: ϕ_{AO} (solid diamonds), ϕ^* (circles), and ϕ_{HS}^{eff} (open diamonds). $q=10$: ϕ_{HS}^{eff} (squares). C denotes the critical point when present. The inset compares $q=5$: ϕ_{AO} (diamonds) and $q=12.5$: ϕ_{AO} (solid triangles) and ϕ_{HS}^{eff} (open triangles).

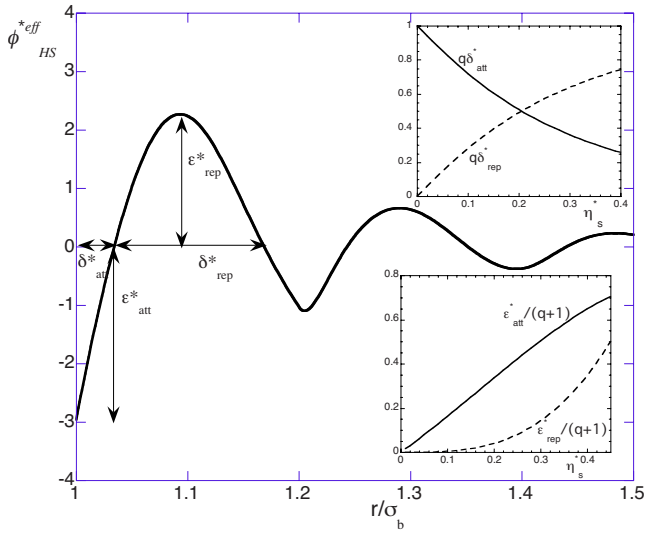

FIG. 5. (Color online) HS mixture effective potential for $q=5$ and $\rho_s^*=0.6$. Insets: variation with $\rho_s^*=0.6$ of the reduced widths δ_{att}^* and δ_{rep}^* (top), and energies ε_{att}^* and ε_{rep}^* (bottom) deduced form the Götzelmann, Evans and Dietrich (GED) potential.

namics [13]. We thus computed the MCT arrest line and the critical points in the plane (η, B_2^r) for some of the situations considered above (Fig. 4) for the potentials ϕ_{AO}, ϕ_{HS}^{eff}, and its truncated version $\phi^*(x \le 1+\delta_{att}^*)=\phi_{HS}^{eff}(x)$ and $\phi^*(x>1+\delta_{att}^*)=0$ (discussed in Sec. IV). The corresponding transition lines differ strongly: while it is almost vertical for $\phi_{AO}(q=5)$, η_g decreases rapidly with B_2^r for ϕ_{HS}^{eff}. These results show that, contrarily to the AO mixture, the HS one does not follow a universal trend even when a global measure of the interaction is used. This also holds for the critical points. In the inset, the comparisons shown for $q=5$ and 12.5 confirm the role of the size asymmetry.

B. Analysis

1. Generic and specific behaviors

To understand these results, one may compare the depletion potentials in the two models in relation with their unique difference: in the AO model, the interaction between the small particles is ignored (ideal depletant) while it is a hard sphere one in the HS mixture. A distinction between universal and specific features can be made by noting first that, in the AO model, the effective potential can be written as $\phi_{AO}=\rho_s^*\psi_q(x)$ with ψ_q independent of ρ_s^* [Eq. (2)]. The "charging" parameter playing the role of the inverse temperature is ρ_s^* and the attraction range $\delta^*=1/q$ (in reduced units) is independent of ρ_s^*. In this case, the generic scenario is expected. In the HS mixture, on the contrary, the effective potential departs from this behavior: when ρ_s^* increases, ϕ_{HS}^{eff} becomes strongly oscillatory with separation (Fig. 5), a consequence of the nonvanishing radius of the small spheres. These well-known oscillations with a periodicity roughly equal to the small spheres diameter reflect increasing short-range correlations between the small particles. The behavior of ϕ_{HS}^{eff} is thus more complex than that described above; in particular, the decoupling between the depth and the width of the attractive well does not hold. Two main features are observed: first, the depletion well close to contact narrows as ρ_s^* increases, for fixed q. Simultaneously, a repulsive barrier develops next to this well, for separations (in units of σ_b) $\delta_{att}^* \le d^* \le \delta_{att}^*+\delta_{rep}^*$ (the other barriers are less important). Since one has roughly $\delta_{att}^*+\delta_{rep}^* \approx 1/q$, the increase in ρ_s^* decreases δ_{att}^* and increases δ_{rep}^*. In addition, the amplitude ε_{rep} of the repulsive barrier increases, too.

The variation of these parameters is illustrated in the inset, using the HS depletion potential derived by Götzelmann *et al.* [56] (see Ref. [27]). When η_s^* increases, ε_{rep} becomes comparable to ε_{att} so that the energy barrier $\varepsilon_{tot}=\varepsilon_{rep}+\varepsilon_{att}$ a particle has to cross to escape from the contact well is significantly greater than ε_{att}. For $q=5$ and $\eta_s^*=0.4$, for example, one has $\varepsilon_{tot} \approx 6kT$, $\varepsilon_{att} \approx 3.9kT$, and $\varepsilon_{AO}=3.6kT$. The variation (inset) of δ_{att}^* and δ_{rep}^* shows that the width δ_{att}^* of the depletion well becomes significantly smaller than $1/q$ for $\eta_s^*>0.2$ (recall that $\delta_{AO}^*=1/q$).

However, this solvent granularity is expected to play a more important role at moderate asymmetry than at very high q (in which case the very narrow and deep well at contact dominates). This explains the following trends:

(i) at high asymmetry the binodals of both models are close to those for very small attraction range ($q>10$): metastable FF transition and coexistence between a low density gas maximizing the entropy and a close-packed solid maximizing the attraction energy. The attractive glass extends to the low density region due to physical bonding [3,6]. However, besides these generic properties, some influence of the granularity of the solvent remains with ϕ_{HS}^{eff} as mentioned previously (in particular, the location of the FF binodal with respect to the FS and the MCT transition lines and the solid-solid transition).

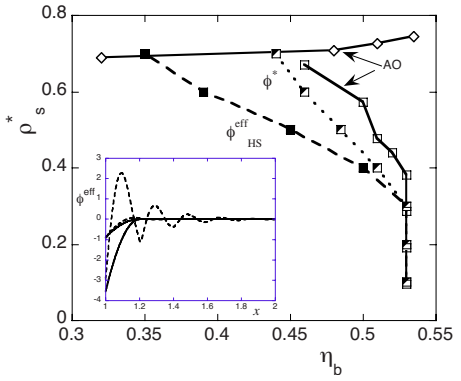

FIG. 6. (Color online) Fluid-fluid and nonergodicity transition lines for $q=5$. ϕ_{HS}^{eff} (solid), ϕ_{AO} (open), and ϕ^* (half filled). The FF binodal exists only for ϕ_{AO}. Inset: ϕ_{AO} (solid line) and ϕ_{HS}^{eff} (dashes) for $\rho_s^*=0.2$ and 0.8.

(ii) for the AO model with moderate asymmetry, the phase diagram observed in Fig. 3(a) follows also the generic behavior: a FF transition, unstable with respect to the FS one when the attraction range is below some critical value ($q_c^{-1} \approx 0.40$ for the AO potential [54,55] and $\kappa_c^{*-1} \approx 0.15$ for the Yukawa potential, with κ^{*-1} as the reduced range [57]). The attractive glass is confined to the dense fluid region. Additionally the binodals are also less flat.

(iii) in HS mixtures with moderate asymmetry, the specificity is manifest. This can be traced back to the quite distinctive features described above, as analyzed now.

2. Moderate asymmetry: Roles of the repulsive barrier and of the attractive well

For checking the influence of the repulsive barrier, we computed the phase diagram for the truncated potential $\phi^*(x \le 1+\delta_{att}^*)=\phi_{HS}^{eff}(x)$ and $\phi^*(x>1+\delta_{att}^*)=0$ (Fig. 6). As with $\phi_{HS}^{eff}(x)$, no FF binodal was observed with ϕ^* for $q=4$ and 5, suggesting that the repulsive barrier has a weak influence on this transition. Both for ϕ^* and ϕ_{HS}^{eff}, the FF transition for $q \le 8$ is absent because the increase in ε_{att} with η_s^* is offset by the rapid decrease in δ_{att}^*, contrarily to ϕ_{AO} for which the width is fixed. On the contrary, the barrier is important for the glass transition, as shown (AO; HS; ϕ^*) in Fig.6. As suggested above, one may anticipate that the barrier stabilizes the physical bonds involved in gelation. The simultaneous decrease in δ_{att}^* with η_s^* reinforces this mechanism (see Secs. IV B and IV C below). The analysis of the B_2 representation shown in Fig. 4 confirms the role of the repulsive barrier distinguishing ϕ_{HS}^{eff} from ϕ^*. Indeed, whereas the attractive well and the barrier both favor gelation, their contributions to B_2 are of opposite sign. However, the difference observed between ϕ^* and ϕ_{AO} shows that the shape of the attractive tail also matters. This shows that nonideal solvent means also nonuniversal features. In this respect it should be stressed that different models may turn out more or less suitable to describe different colloidal systems. For instance, the AO-like models without repulsive barriers should be appropriate to globular proteins or polymer-colloid mixtures

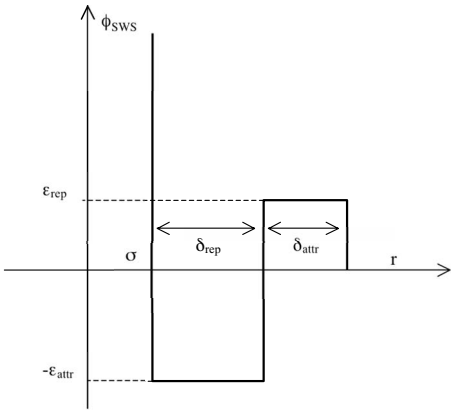

FIG. 7. Square well and shoulder potential.

whereas the oscillatory depletion potential is expected to correspond more to mixture of hard-sphere-like colloids.

IV. SQUARE WELL AND SHOULDER POTENTIAL

As discussed in the previous section, the features of the effective potentials such as the depth at contact, the amplitude of the oscillations, etc.—which are responsible for the departure from the generic scenario—change in a complex way with the "control" variables, q and ρ_s^*. In order to distinguish between the different effects, we consider here the "square well and shoulder" potential (ϕ_{SWS}), in which these features can be varied separately. The relevant parameters are defined in Fig. 7.

A. Gelation versus fluid-fluid transition

The FF critical point and the glass transition line were computed in the (η, T^*) plane (with η the packing fraction and T^* the reduced temperature kT/ε_{att}) for various values of δ_{att}^* (width of the attractive well) and of δ_{rep}^* (width of the shoulder) and of the ratio $\varepsilon_{rep}/\varepsilon_{att}$ (hereafter, the lengths are in units of δ and the energies are in units of k_BT). Although ϕ_{SWS} may only grossly mimic the actual effective potential, we have considered some values typical of this potential for the asymmetry range considered here: for example, the widths $\delta_{att}^*=0.03$, 0.06, and 0.1 and $\delta_{rep}^*=2.33\delta_{att}^*$ correspond roughly to those found for $\eta_s^* \approx 0.35$ and $q \approx 10$, 5, 3, respectively. The variation with δ_{att}^* and δ_{rep}^* is first presented in Fig. 8 for $\delta_{att}^*=0.03$, 0.1, and in each case, $\delta_{rep}^*=0$, δ_{att}^*, $2.33\delta_{att}^*$ ($\delta_{rep}^*=0$: SW potential). In all these figures $\varepsilon_{rep}/\varepsilon_{att}=1$ for simplicity. The influence of $\varepsilon_{rep}/\varepsilon_{att}$ is next illustrated in the inset for $\delta_{rep}^*=\delta_{att}^*=0.1$. For $\delta_{att}^*=0.1$ the MCT line cannot be computed at large ε_{att}^* because the nonconvergence region of the RHNC equation then precludes the computation of the static structure factor.

Considering first the case $\delta_{rep}^*=0$, one recovers the pattern obtained for the SW or other similar short-range potentials [3,4,11]: decreasing the attraction range favors equilibrium gelation, in the MTC treatment, by pushing the critical point toward higher values of ε_{att}^*. As shown in the inset of Fig. 8(a), for $\delta_{att}^*=0.03$, our MCT results are very close to those obtained by Foffi *et al.* in [58]. These situations are precisely

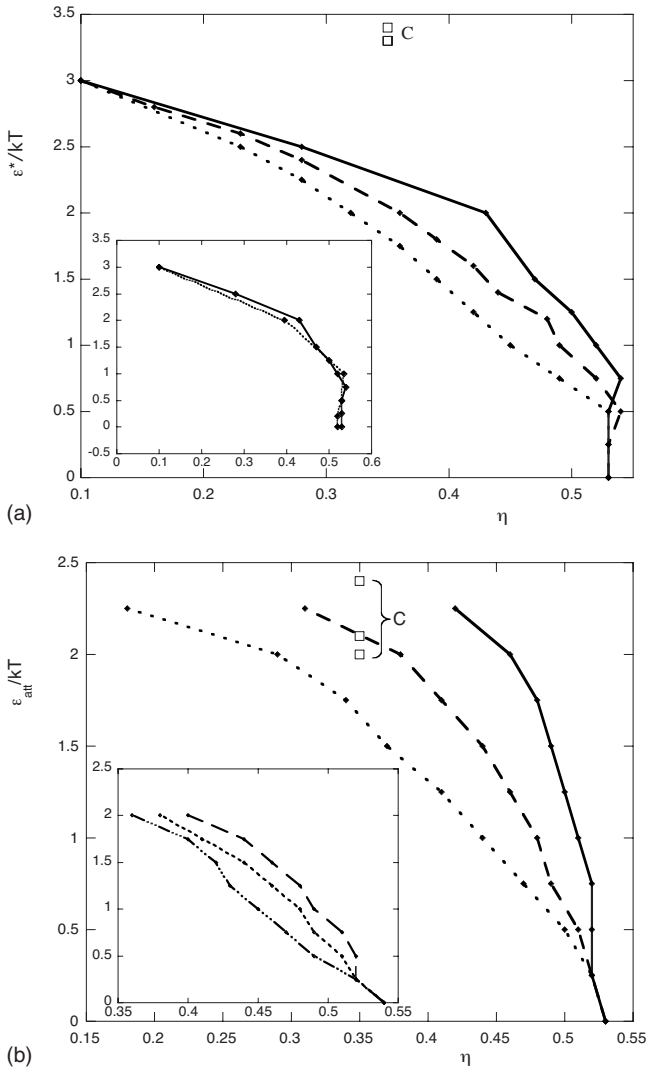

FIG. 8. Nonergodicity transition lines and FF critical point (C) for the SWS potential for (a) $\delta^*_{att}=0.03$ and (b) $\delta^*_{att}=0.1$, with $\varepsilon_{rep}/\varepsilon_{att}=1$. Solid line: $\delta^*_{rep}=0$. Dashes: $\delta^*_{rep}=\delta^*_{att}$. Dots: $\delta^*_{rep}=2.3\delta^*_{att}$. For the FF critical points (C: squares), ε_{att}/k_BT_c increases with δ_{rep}. Inset (a): comparison with [55] (dots) for $\delta^*_{rep}=0$. Inset (b): nonergodicity line for $\delta^*_{rep}=\delta^*_{att}$, and $\varepsilon_{rep}=\varepsilon_{att}/2$ (long dashes), $\varepsilon_{rep}=\varepsilon_{att}$ (short dashes), and $\varepsilon_{rep}=2\varepsilon_{att}$ (dots and dashes) (the FF critical point does not vary).

those for which the MCT results have been questioned on the basis of subsequent molecular-dynamics simulations [18].

The addition of a repulsive barrier favors then systematically gelation at lower density and pushes simultaneously the critical point at higher ε^*_{att}. However, these effects have quite different amplitudes according to δ^*_{att} and the considered transition. (i) The displacement of the critical point is weaker than that of the glass transition line. This confirms the trends observed for the HS effective potential. (ii) The effect of the repulsive barrier is the strongest when the attraction range is not too small. For $\delta^*_{att}=0.03$, indeed, the location of the critical point is almost unaffected by the repulsive barrier, even when $\delta^*_{rep}=\delta^*_{att}$, and the MCT line is only moderately shifted (low density gelation is in turn observed regardless of the presence of the barrier). At the attraction width, $\delta^*_{att}=0.1$, the phase behavior is qualitatively modified by the introduction of the repulsive barrier: low density gelation is indeed observed only when it is present. Furthermore, the location of the MCT line is sensitive to its width. In accordance with the rough correspondence made above between ϕ_{SWS} and ϕ^{eff}_{HS}, these features are consistent with the behavior observed for the actual depletion potential, for which two situations have also been evidenced, depending on the size ratio. One recovers also the differences between the MCT lines computed for ϕ^{eff}_{HS} and the truncated potential ϕ^* for $q=5$. The principal difference is however that a critical point is always present for ϕ_{SWS} since the range and the charging parameter are then independent. Like for δ^*_{rep}, the effect of increasing the repulsive energy ε^*_{rep} (for fixed values of δ^*_{rep} and δ^*_{att}) is also to shift the nonergodicity line toward lower densities [inset of Fig. 8(b)]. The critical point is not modified. Finally, we have also computed the nonergodicity transition lines in the (η, B_2) plane: they do not follow a universal behavior, like for ϕ^{eff}_{HS}.

B. Localization length

The transition from a repulsive to an attractive glass can be identified from the changes observed in the long-time limit of the density autocorrelation function f_q or alternatively in the self-particle-contribution f^s_q [3]. It leads to a strong decrease in the particle localization length r_{loc}, which is usually interpreted as the consequence of the formation of bonds between the particles due to the attractive forces. The contribution of the repulsive barriers to bonding was then checked in [21], by comparing the variations of r_{loc} associated with ϕ^{eff}_{HS} and with its truncated version ϕ^*. However, r_{loc} was computed for these two potentials along there respective line of arrest. For more evocative comparisons, r_{loc} is computed here for different SWS potentials at the same points of the phase diagram. We compare in this way the localization radii corresponding to ϕ_{SWS} with the same attractive part but different repulsive barriers, along the MCT line computed for the pure SW, $\varepsilon^*_{rep}=0$ (Fig. 9). This is done for $\delta^*_{att}=0.1$, in the simplest Gaussian approximation [10]. The effect on r_{loc} of the repulsive barrier is clearly evidenced: in the attractive glass observed for $\varepsilon^*_{att}>05$, the value r_{loc} is almost divided by 2 for $\varepsilon^*_{rep}=\varepsilon^*_{att}$ and $\delta^*_{att}=0.23$ (which would correspond roughly to $\eta^*_s\approx 0.35$ for ϕ^{eff}_{HS}). We note that the variation with the physical parameters is nonlinear since it seems to saturate at large ε^*_{rep} and δ^*_{rep}, and that these two parameters play a similar role.

C. Escape time at infinite dilution

Additional insight on the stabilizing effect of a repulsive barrier on the bonding mechanism involved in gelation is provided by the time τ_{esc} for a Brownian particle to escape from the potential (the particle being located initially at the potential-energy minimum). From this definition, τ_{esc} can be regarded as the bond lifetime between two interacting particles in the dilute fluid regime. It should of course not be confused with the bond lifetime in the gel state since the latter depends also on the dynamical correlations with the

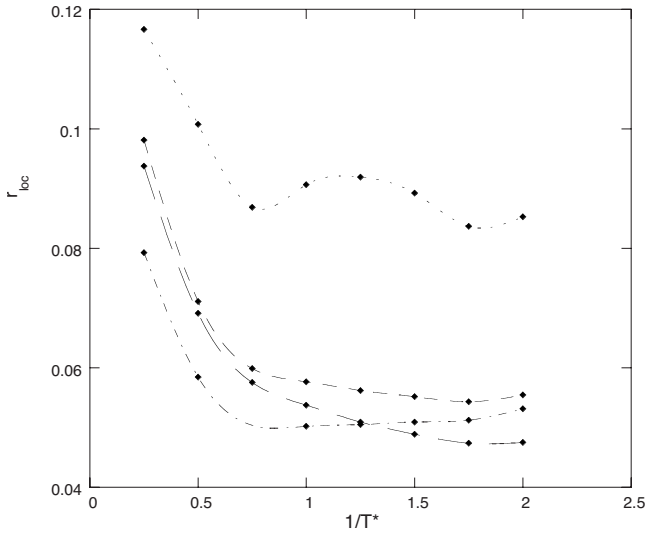

FIG. 9. Variation with T^* of the particle localization length in the nonergodic state for SWS potentials with $\delta^*_{att}=1$. Dots: $\varepsilon_{rep}=0$; dashes: ($\varepsilon_{rep}=\varepsilon_{att}$, $\delta^*_{rep}=\delta^*_{att}$); long dashes: ($\varepsilon_{rep}=\varepsilon_{att}$, $\delta^*_{rep}=2.3\delta^*_{att}$); dot and dashes: ($\varepsilon_{rep}=2\varepsilon_{att}$, $\delta^*_{rep}=\delta^*_{att}$).

other particles. However, one may expect similar effects of the attraction and repulsion parameters on these different times, at least qualitatively. The escape time τ_{esc} can be computed from Kramer's expression [59] for a potential having the characteristics of those investigated here: a deep well and a repulsive barrier between the well and the free particle region, both having a characteristic energy greater than k_BT (this is different from the considerations on the Asakura-Oosawa potential in [60]). From these assumptions, τ_{esc} writes

$$\tau_{esc}=\frac{1}{D_0}\int_0^{\delta_{att}+\delta_{rep}} dx'\ e^{\beta\phi_{\mathrm{SWS}}(x')}\int_{-\infty}^{x'} dx\ e^{\beta\phi_{\mathrm{SWS}}(x)}, \quad (5)$$

which leads to the following expression for the SWS potential:

$$\tau_{esc}=\frac{1}{D_0}\{(\delta_{att}+\delta_{rep})^2+\delta_{att}\delta_{rep}(e^{\varepsilon^*_{att}+\varepsilon^*_{rep}}-1)\}. \quad (6)$$

In Eq. (6), D_0 is the free particle diffusion coefficient (in the absence of hydrodynamic interactions). This expression is qualitatively consistent with the stabilizing effect of δ^*_{rep} and ε^*_{rep} on the gel transition line and the particle localization as measured by r_{loc}. Concerning τ_{esc}, this can be understood from considerations on the probabilities for the Brownian particle to overcome the energy barrier $\varepsilon^*_{att}+\varepsilon^*_{rep}$ (which is enhanced by ε^*_{rep}), and next jump across the barrier width δ^*_{rep} without coming back in the well (a similar expression can be found in [61]. However, it is difficult to make a more precise correlation: for example, the simple behavior in $(\varepsilon^*_{att}+\varepsilon^*_{rep})$ obtained for τ_{esc} does not hold for the gel properties [compare, e.g., in the inset of Fig. 8(b) the gel transition packing fractions for $(\varepsilon^*_{att},\varepsilon^*_{rep})=(2,1)$ and (1.5,1.5)]. Also the influence of δ^*_{rep}, with respect to that of ε^*_{rep}, is weaker for τ_{esc} than for the gel properties (replacing the pair potential with the mean force one $-kT\ln[g(r)]$ at finite density does not seem to restore the influence of δ^*_{rep}).

V. MIXTURES OF HARD-SPHERE-LIKE COLLOIDS

To deepen this question of specificity, in relation with a finer description of the interactions, we finally consider binary mixtures of hard particles, with residual *direct* interactions between the particles. This will give an idea of the scenarios one may actually observe with real mixtures. As well known, the HS model is used when the actual potentials vary on a very short range with respect the size of the particles and is weak beyond the steep repulsion ("HS-like particles"). While this modeling has proven reasonable for monodisperse suspensions (see, e.g., [62–65].), it is more disputable for pseudobinary mixtures. In [39] we have shown indeed that the incorporation of moderate attractions with very short range, at the scale of the small colloids, can modify the binodals at the qualitative level, for $q=10$ (this is different from the situations discussed in Sec. III B 1 in which only hard-sphere interactions were present). Using the HS mixture as a reference system for highly asymmetric mixture may thus also be questioned [66]. We thus include in this section the effect of similar residual interactions on the nonergodicity transition lines of mixtures of HS-like particles for $q=5$ and 10. In both cases, the residual interaction is a Yukawa attraction between unlike particles,

$$\beta u_{sb}(r>\sigma_{sb})=\frac{\varepsilon^*}{r/\sigma_{sb}}\exp\left\{-\frac{(\sigma_{sb}-r)}{\xi_{sb}}\right\}, \quad (7)$$

where $\sigma_{sb}=(\sigma_s+\sigma_b)/2$ and $\sigma_{s,b}$ is the small (big) particle diameter. We take $|\varepsilon^*|=1.5$, and the range ξ_{sb} is chosen so that the interaction is truly "residual:" $\xi_{sb}/\sigma_s=[\frac{1}{100},\frac{1}{40}]$. This corresponds to a relative deviation $\Delta B^{(2)}_{sb}=(B^{(2)}_{sb}-B^{(2)}_{sb,HS})/B^{(2)}_{sb,HS}$ of the second virial coefficient $\Delta B^{(2)}_{sb}=-1.3\%$ to -3.1% for $q=10$, for example (see Ref. [39] for details).

We recall that for $q\sim 5$, $\varepsilon^*=\pm 1.5$, and $\xi_{sb}=\sigma_s/100$, we found [21] that gelation occurs without the competition with the FF transition, both for the pure HS mixture and that with residual interactions (Fig. 10). The effect of the residual interaction is indeed observable only on the MCT line, and it is weaker in this case than for $q=10$ and the same value of ξ_{sb}/σ_s (inset). Since this model seems closer to reality, one may expect equilibrium gelation in a significant number of mixtures of HS-like particles with similar size ratios.

We finally present the phase diagram of a mixture with $q=10$, $\varepsilon^*=-1.5$, and $\xi_{sb}=\sigma_s/40$ ($\Delta B^{(2)}_{sb}=-3.1\%$), as an illustrative example of the variety of possible behaviors (Fig. 11). The noteworthy features are no FF binodal, spectacular extension of the homogenous fluid phase, re-entrance of the crytallization line, nonergodic fluid out of the FS coexistence domain, widening of the FS coexistence domain at higher density of small particles, and isostructural SS transition. These properties are of course related to the specificities of the effective potential (inset) in this situation. Concerning the binodals, the principal cause is the strong reduction in the depletion well at contact, $\phi^{eff}(\sigma_b)$, induced by the residual

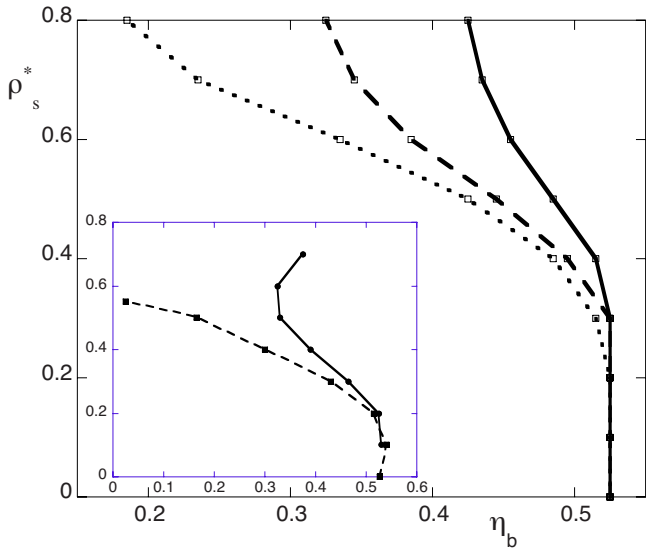

FIG. 10. (Color online) Nonergodicity transition lines of a mixture of hard-sphere-like particles for $q=5$ and $\xi_{sb}=\sigma_{sb}/100$. Dashes: pure hard spheres; dots: $\varepsilon_{sb}=+\frac{3}{2}k_BT$ (with ε_{sb} as the contact value); solid line: $\varepsilon_{sb}=-\frac{3}{2}k_BT$. Inset: $q=10$. Dashes: pure hard spheres; solid line: $\varepsilon_{sb}=-\frac{3}{2}k_BT$.

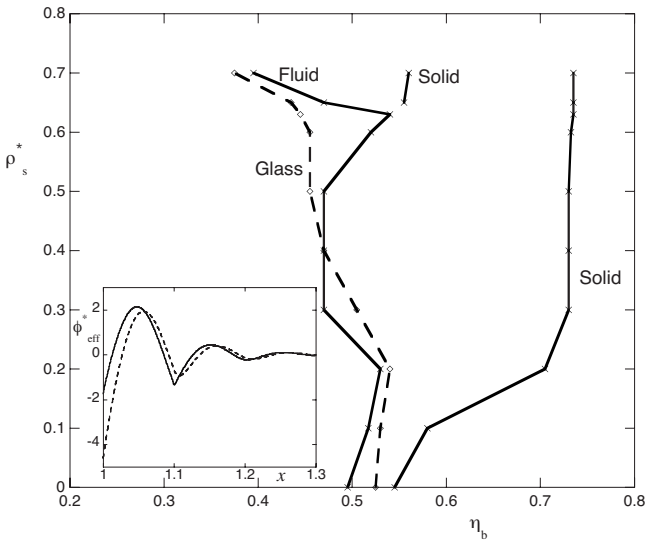

FIG. 11. Phase diagram of a mixture of hard-sphere-like particles for $q=10$, $\xi_{sb}=\sigma_{sb}/40$, and $\varepsilon_{sb}=-\frac{3}{2}k_BT$. Solid line: binodals; dashes: nonergodicity transition line. Inset: corresponding effective potential for $\rho_s^*=0.6$.

attractions (see the inset). Due to the correlations between the small particles, $\phi^{eff}(\sigma_b)$ varies in a nonmonotonic way with ρ_s^*. This leads to a re-entrant behavior. The widening of the FS coexistence domain at higher small particle density, together with the SS transition, is then associated with the deepening of a second minimum in the potential at $r=\sigma_b+\sigma_s$, with the big-small sphere attraction bridging the big particles.

Concerning the nonergodicity transition, the reduction in the depth of the depletion well with respect to ϕ_{HS}^{eff} proves less influential than for the crystallization line: in particular no re-entrance is observed even when $|\phi^{eff}(\sigma_b)|$ decreases with ρ_s^*, due to the simultaneous increase in the height of the repulsive barrier. Although one cannot ascertain that this particular pattern will actually be observed due to the great sensitivity, at high asymmetry, of the transition lines to other details of the interactions, this example illustrates the possibility of specific behaviors, well beyond the generic scenario.

VI. CONCLUSION

We have analyzed the interplay between gelation and equilibrium phase transitions in asymmetric mixtures of hard-sphere-like colloids, in the effective one-component approximation. In this representation, the big particles interact through a short-range effective interaction, which is mediated by the small spheres. One main feature of the effective potential in hard-sphere mixtures is the presence of an attractive part in a narrow range close to contact, such as in colloid-polymer ones or other suspensions. This is expected to favor the onset of attractive glasses or gels whose interplay with the equilibrium fluid condensation is the subject of vivid debates. We have analyzed for these mixtures the validity of the generic scenario drawn from standard potentials composed of a hard core plus a short-range effective attraction, according to which gelation is related to fluid-fluid phase separation. We have shown that contrarily to the Asakura-Oosawa potential, which assumes an ideal depletant, strong specificities are associated with the nonzero correlations between the smaller particles in actual pseudobinary mixtures. This is related to the fine structure of the oscillatory effective potential whose variations with the physical parameters are much more complex than for standard potentials. These specificities of the effective potential influence differently the FF and the nonergodicity transition line. As the principal consequence, we predict equilibrium gelation *without* the competition with the fluid-fluid transition in mixtures of hard-sphere-like colloids with moderate size ratios (typically $q\sim 4-8$). It will be observed provided that crystallization is inhibited by a sufficient degree of polydispersity. We have also shown that, at higher asymmetry, the residual non-hard-sphere interactions—which exist in real mixtures of hard-sphere-like particles—can strongly modify the phase diagram with respect to the pure HS situation. This leads to a rich variety of behaviors, well beyond the generic scenario, according to the details of the interactions between the components of the mixture. Since such details may be important, it might be necessary to assess the different modeling steps leading to the effective one-component representation. A possible comparison with measured effective potentials—for the same state points used to draw the phase diagram—would hence be useful. These observations should stimulate further experimental investigations on these systems. In the future, numerical simulations should also be useful to quantify more precisely the qualitative trends discussed in this paper. Work is in progress in this direction.

[1] W. Götze, in *Liquids, Freezing and Glass Transition*, edited by J.-P. Hansen, D. Levesque, and J. Zinn-Justin (North-Holland, Amsterdam, 1991), pp. 287–350.
[2] G. Szamel and H. Löwen, Phys. Rev. A **44**, 8215 (1991).
[3] J. Bergenholtz and M. Fuchs, Phys. Rev. E **59**, 5706 (1999); J. Phys.: Condens. Matter **11**, 10171 (1999).
[4] K. A. Dawson, G. Foffi, F. Sciortino, P. Tartaglia, and E. Zaccarelli, J. Phys.: Condens. Matter **13**, 9113 (2001).
[5] K. N. Pham *et al.*, Science **296**, 104 (2002); K. N. Pham, S. U. Egelhaaf, P. N. Pusey, and W. C. K. Poon, Phys. Rev. E **69**, 011503 (2004).
[6] J. Bergenholtz, W. C. K. Poon, and M. Fuchs, Langmuir **19**, 4493 (2003).
[7] G. Foffi, K. A. Dawson, S. V. Buldyrev, F. Sciortino, E. Zaccarelli, and P. Tartaglia, Phys. Rev. E **65**, 050802(R) (2002).
[8] A. M. Puertas, M. Fuchs, and M. E. Cates, Phys. Rev. Lett. **88**, 098301 (2002); Phys. Rev. E **67**, 031406 (2003).
[9] Emanuela Zaccarelli, Francesco Sciortino, and Piero Tartaglia, J. Phys.: Condens. Matter **16**, S4849 (2004).
[10] Y. L. Chen and K. S. Schweizer, J. Chem. Phys. **120**, 7212 (2004).
[11] D. C. Viehman and K. S. Schweizer, J. Chem. Phys. **128**, 084509 (2008).
[12] K. Dawson, Curr. Opin. Colloid Interface Sci. **7**, 218 (2002).
[13] E. Zaccarelli, J. Phys.: Condens. Matter **19**, 323101 (2007).
[14] N. M. Dixit and C. F. Zukoski, Phys. Rev. E **67**, 061501 (2003).
[15] F. Cardinaux, T. Gibaud, A. Stradner, and Peter Schurtenberger, Phys. Rev. Lett. **99**, 118301 (2007).
[16] M. C. Grant and W. B. Russel, Phys. Rev. E **47**, 2606 (1993).
[17] T. Eckert and E. Bartsch, Phys. Rev. Lett. **89**, 125701 (2002).
[18] G. Foffi, C. De Michele, F. Sciortino, and P. Tartaglia, Phys. Rev. Lett. **94**, 078301 (2005); J. Chem. Phys. **122**, 224903 (2005).
[19] F. Sciortino, Eur. Phys. J. B **64**, 505 (2008).
[20] E. Zaccarelli, P. J. Lu, F. Ciulla, D. Weitz, and F. Sciortino, J. Phys.: Condens. Matter **20**, 494242 (2008).
[21] Ph. Germain and S. Amokrane, Phys. Rev. Lett. **102**, 058301 (2009).
[22] P. J. Lu, E. Zaccarelli, F. Ciulla, A. B. Schofield, F. Sciortino, and D. A. Weitz, Nature (London) **453**, 499 (2008).
[23] M. Noro and D. Frenkel, J. Chem. Phys. **113**, 2941 (2000).
[24] B. Ruzicka, L. Zulian, R. Angelini, M. Sztucki, A. Moussaïd, and G. Ruocco, Phys. Rev. E **77**, 020402(R) (2008).
[25] S. Ramakrishnan, M. Fuchs, K. S. Schweizer, and C. F. Zukoski, J. Chem. Phys. **116**, 2201 (2002).
[26] S. A. Shah, Y.-L. Chen, K. S. Schweizer, and F. C. Zukoski, J. Chem. Phys. **119**, 8747 (2003).
[27] Ph. Germain and S. Amokrane, Phys. Rev. E **76**, 031401 (2007).
[28] M. Dijkstra, R. van Roij, and R. Evans, Phys. Rev. E **59**, 5744 (1999).
[29] N. G. Almarza and E. Enciso, Phys. Rev. E **59**, 4426 (1999).
[30] J. Clement-Cottuz, S. Amokrane, and C. Regnaut, Phys. Rev. E **61**, 1692 (2000).
[31] J.-G. Malherbe and S. Amokrane, Mol. Phys. **99**, 355 (2001).
[32] A. Ayadim and S. Amokrane, Phys. Rev. E **74**, 021106 (2006).
[33] S. Amokrane, A. Ayadim, and J. G. Malherbe, J. Phys.: Condens. Matter **15**, S3443 (2003).
[34] T. L. Hill, *Statistical Mechanics* (Dover, New York, 1987).
[35] J. P. Hansen and I. R. Mc Donald, *Theory of Simple Liquids* (Academic, New York, 1986).
[36] F. Lado, S. M. Foiles, and N. W. Ashcroft, Phys. Rev. A **28**, 2374 (1983).
[37] Y. Rosenfeld, J. Chem. Phys. **98**, 8126 (1993).
[38] S. Amokrane and J. G. Malherbe, J. Phys.: Condens. Matter **13**, 7199 (2001); **14**, 3845(E) (2002).
[39] Ph. Germain, J. G. Malherbe, and S. Amokrane, Phys. Rev. E **70**, 041409 (2004).
[40] S. Asakura and F. Oosawa, J. Chem. Phys. **22**, 1255 (1954).
[41] A. Vrij, Pure Appl. Chem. **48**, 471 (1976).
[42] A. Malijevsky and S. Labik, Mol. Phys. **60**, 663 (1987); S. Labik and A. Malijevski, *ibid.* **67**, 431 (1989).
[43] M. Hasegawa, J. Chem. Phys. **108**, 208 (1998).
[44] W. Götze and L. Sjögren, J. Math. Anal. Appl. **195**, 230 (1995).
[45] U. Bengtzelius, W. Götze, and A. Sjölander, J. Phys. C **17**, 5915 (1984).
[46] W. Götze and L. Sjögren, Phys. Rev. A **43**, 5442 (1991); Rep. Prog. Phys. **55**, 241 (1992).
[47] W. van Megen and S. M. Underwood, Phys. Rev. Lett. **70**, 2766 (1993); Phys. Rev. E **49**, 4206 (1994).
[48] E. Zaccarelli *et al.*, Phys. Rev. Lett. **95**, 268301 (2005).
[49] E. Zaccarelli, H. Löwen, P. P. F. Wessels, F. Sciortino, P. Tartaglia, and C. N. Likos, Phys. Rev. Lett. **92**, 225703 (2004).
[50] G. A. Vliegenthart and P. van der Schoot, EPL **62**, 600 (2003).
[51] A. Imhof and J. K. G. Dhont, Phys. Rev. Lett. **75**, 1662 (1995); Phys. Rev. E **52**, 6344 (1995).
[52] A. Fortini, E. Sanz, and M. Dijkstra, Phys. Rev. E **78**, 041402 (2008).
[53] S. Babu, J.-C. Gimel, and T. Nicolai, J. Chem. Phys. **130**, 064504 (2009).
[54] E. J. Meijer and D. Frenkel, J. Chem. Phys. **100**, 6873 (1994).
[55] M. Dijkstra, J. M. Brader, and R. Evans, J. Phys.: Condens. Matter **11**, 10079 (1999).
[56] B. Götzelmann, R. Evans, and S. Dietrich, Phys. Rev. E **57**, 6785 (1998).
[57] M. H. J. Hagen and D. Frenkel, J. Chem. Phys. **101**, 4093 (1994).
[58] G. Foffi, G. D. McCullagh, A. Lawlor, E. Zaccarelli, K. A. Dawson, F. Sciortino, P. Tartaglia, D. Pini, and G. Stell, Phys. Rev. E **65**, 031407 (2002).
[59] H. A. Kramers, Physica (Amsterdam) **7**, 284 (1940).
[60] M. Laurati, G. Petekidis, N. Koumakis, F. Cardianux, A. B. Scofield, J. M. Brader, M. Fuchs, and S. U. Egelhaaf, J. Chem. Phys. **130**, 134907 (2009).
[61] J. L. Barrat and J. P. Hansen, *Basic Concepts for Simple and Complex Fluids* (Cambridge University Press, Cambridge, England, 2003).
[62] A. D. Dinsmore, A. G. Yodh, and D. J. Pine, Phys. Rev. E **52**, 4045 (1995).
[63] W. C. Poon, J. Phys.: Condens. Matter **14**, R859 (2002).
[64] G. Bryant, S. R. Williams, Q. Lin Mao, I. K. Snook, E. Perez, and F. Pincet, Phys. Rev. E **66**, 060501(R) (2002).
[65] A. Yethiraj and A. van Blaaderen, Nature (London) **421**, 513 (2003).
[66] Ph. Germain, C. Regnaut, and S. Amokrane, Phys. Rev. E **67**, 061101 (2003).